

# Radiofrequency multipole traps: Tools for spectroscopy and dynamics of cold molecular ions

**Roland Wester**

Department of Physics, University of Freiburg, Hermann-Herder-Str. 3, 79104 Freiburg, Germany

E-mail: [roland.wester@physik.uni-freiburg.de](mailto:roland.wester@physik.uni-freiburg.de)

**Abstract.** Multipole radiofrequency ion traps are a highly versatile tool to study molecular ions and their interactions in a well-controllable environment. In particular the cryogenic 22-pole ion trap configuration is used to study ion-molecule reactions and complex molecular spectroscopy at temperatures between few Kelvin and room temperatures. This article presents a tutorial on radiofrequency ion trapping in multipole electrode configurations. Stable trapping conditions and buffer gas cooling, as well as important heating mechanisms, are discussed. In addition, selected experimental studies on cation and anion-molecule reactions and on spectroscopy of trapped ions are reviewed. Starting from these studies an outlook on the future of multipole ion trap research is given.

Submitted to: *J. Phys. B: At. Mol. Phys.*

## 1. Introduction

Advances in our understanding of the structure and dynamics of small quantum systems is closely related to improved techniques to prepare such systems in well-controlled quantum states. Particle traps that confine atoms, molecules or clusters for a long time are essential tools for this. Traps for charged particles, in particular the radiofrequency Paul trap [1, 2] and the electromagnetic Penning trap [3], have been introduced many years ago. Two newer trap designs have been developed recently. The electrostatic resonator Zajfman trap has been introduced as a tool to study interactions of trapped ions in motion [4] and the Orbitrap has been developed as a versatile high-resolution mass spectrometer [5]. Ion traps find many applications, among them mass spectrometry [6, 7], precision spectroscopy [8, 9], and the implementation of quantum logic [10]. Multipole radiofrequency ion traps, the topic of this article, are widely used to control trapped molecular systems that have many degrees of freedom [11]. The spectroscopy and reactivity of molecular ions is studied in these traps to unravel their dynamics [12, 13] and simulate the properties of cold plasmas, such as the Earth's atmosphere or the interstellar medium [14].

Radiofrequency ions traps have effective trap depths of the order of 1 eV, in contrast to traps for neutral atoms or molecules, which are based on interactions of the electric or magnetic dipole moment or the electric polarizability and are typically of the order of  $10^{-4}$  to  $10^{-7}$  eV [15]. This implies that ions that carry a significant amount of kinetic energy can still be trapped. Different approaches exist to cool trapped ions, collisional cooling with a surrounding neutral buffer gas [3], laser-cooling on a suitable optical transition [16], and - as a combination of these two - sympathetic cooling with jointly trapped laser-cooled ions [17]. Direct laser cooling of molecules with their manifold of internal quantum states is not possible due to the lack of a closed optical cycling transition. Therefore either the first or the third method is employed to cool *molecular ions*.

The technique of sympathetic cooling of molecular ions with laser-cooled atomic ions in a joint quadrupole ion trap has been introduced only a few years ago [18, 19, 20]. It has been successfully used to cool the translational motion of trapped molecular ions down to temperatures of a few millikelvin. These extremely cold and localized ions are well suited for photodissociation experiments [21, 22] and for precision spectroscopy [23]. However, ion-ion collisions have been found to leave the internal quantum state distribution unchanged [24, 25] and are thus not useful for rovibrational cooling of trapped molecular ions. As an alternative, an optical pumping scheme has been proposed to cool internal degrees of freedom [26]. Recently, first reaction experiments with sympathetically cooled molecular ions have been reported using room temperature neutral reactants [27, 28], and - in combination with electrostatically filtered molecules - at relative energies corresponding to about one Kelvin [29, 30].

In the main part of this article the focus will be on collisional cooling with a cold neutral buffer gas. In contrast to sympathetic ion-ion cooling this approach allows one to cool the translational motion as well as the internal rovibrational degrees of freedom at the same time. With helium as the buffer gas, translational and internal temperatures down to a few Kelvin are reached (see section 3). Details of the interaction of the molecular ion with the helium, such as inelastic collision cross sections, determine the time scale for buffer gas cooling but do not inhibit the application in principle. This technique is therefore applicable to essentially all

stable molecular ions over a wide range of temperatures. In addition, neutral collision partners for chemical reactions are also thermalized to the same temperature. Buffer gas cooling therefore provides good starting conditions for a variety of experiments on ion-neutral reactions and laser spectroscopy under controlled thermal conditions (see sections 5 and 6).

As explained in section 3, buffer gas cooling works best if the interaction of the ion with the confining electric field of the radiofrequency trap is limited to a minimum. This obvious contradiction is resolved by trapping in higher-order radiofrequency multipole configurations. These offer a suppressed electric field in the center of the trap and an effective potential that increases much more steeply than the harmonic potential of a quadrupole or Paul ion trap. In this way the confinement in a multipole ion trap comes close to the particle-in-a-box situation with ions moving in an almost field-free volume bound by steep potential walls.

The application of higher order radiofrequency multipole structures for the confinement of charged particles dates back to the 1970ies when the first experiments with radiofrequency multipole ion guides were reported [31]. The two-dimensional confinement in ion guides allowed precise studies of ion-molecule collision cross sections at relative energies between a few meV and several eV. This has developed into a widely used method up to the present day [32]. Three-dimensional confinement in multipole structures has been introduced about a decade later. In octupole ion traps experiments with laser-cooled ions have been carried out to image the ion density by spatially resolving the fluorescence signal [33, 34]. More recently, novel ring-shaped and cylindrical crystals made of laser-cooled ions have been studied in an octupole ion trap [35]. The first ion trap with a large field-free region that was employed in experiments was the ring electrode trap [36], which could already be cooled to liquid nitrogen temperature. This led to extended interaction times of the trapped ions of many seconds instead of just microseconds. Thereby processes that occur with very small cross sections could be studied. With the development of improved cryogenic ion traps, in particular the 22-pole ion trap [37], processes such as radiative association [38] and three-body, complex-forming collisions [39, 40] could be studied at low temperature. This also made it possible to investigate low-temperature reactions that are relevant for the understanding of the interstellar medium. In the last ten years the 22-pole ion trap has become increasingly popular to study ion-molecule reactions and molecular ion spectroscopy.

The concepts of ion guiding and trapping with multipole fields have been discussed extensively in a landmark review by Gerlich in 1992 [11]. Since then major developments have happened, most notably the introduction of the widely used 22-pole ion trap [37]. More recently, a few overview articles have reviewed multipole ion traps [41, 42] and their application in mass spectrometry [7] and astrophysics [43, 14].

This tutorial on multipole rf ion traps starts out presenting the concept of trapping in high-order multipole fields (next section), followed by a discussion of ion cooling with buffer gas (section 3). Then the typically employed experimental techniques are described (section 4). The next two sections are devoted to the two major research areas in which multipole ion traps are used, cold ionic reactions (section 5) and spectroscopy of internally cold ions (section 6). The outlook (section 7) highlights several interesting directions that are currently coming into the focus of this research.

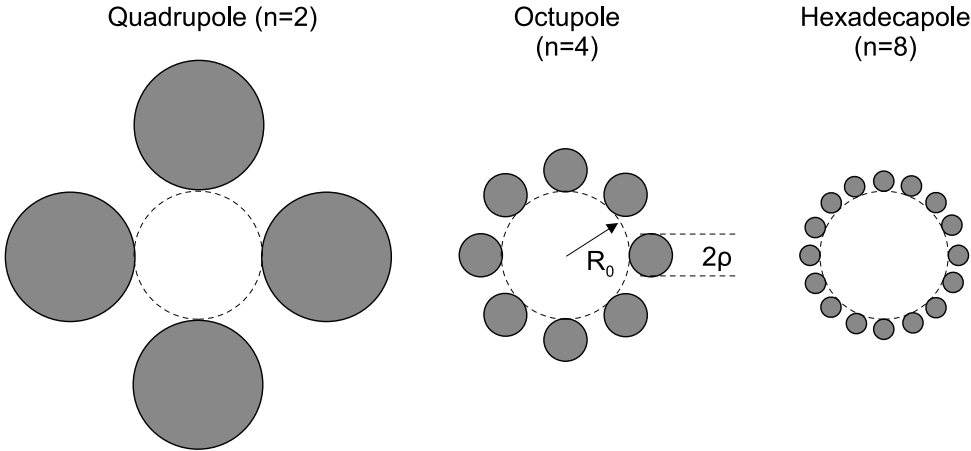


**Figure 1.** Cross sections through three different linear radiofrequency multipole structures of order  $n = 2, 4$  and  $8$ . All multipoles are approximated by  $2n$  cylindrical rods of optimal diameter (see Eq. 2).

## 2. Trapping ions in high-order multipole fields

### 2.1. The effective potential approximation

Multipole ion traps and ion guides typically employ linear radiofrequency electrode geometries that follow a discrete cylindrical symmetry. The time-varying electric potential of an ideal two-dimensional multipole configuration of order  $n$  with infinite extension along the  $z$ -direction is given in cylindrical coordinates by

$$V(r, \phi, t) = V_0 \cos(n\phi) \left( \frac{r}{R_0} \right)^n \sin(\omega t), \quad (1)$$

where  $V_0$  is the radiofrequency amplitude,  $R_0$  the inscribed radius of the rf electrodes (see Fig. 1) and  $\omega$  denotes the angular frequency. In practice, this potential is created by  $2n$  cylindrical electrodes of radius  $\rho$  arranged on a cylinder of inscribed radius  $R_0$ , as shown in Fig. 1 for several different multipole orders  $n$ . To achieve a potential that optimally approximates the curvature of the ideal multipole potential of Eq. 1 to first and second order, the diameter of the rods has to fulfill the relation [11]

$$\rho = \frac{R_0}{n-1}. \quad (2)$$

For a trap diameter of  $2R_0 = 10$  mm and a rod diameter of  $2\rho = 1$  mm this leads to  $n = 11$ , the widely-used 22-pole ion trap.

The dynamics of ions in the time-dependent field of a multipole ion trap can not be solved analytically, in contrast to the dynamics in a quadrupole or Paul trap, because the equation of motion becomes non-linear in the position coordinate. Instead, the best way to describe the dynamics is with the aid of the effective potential approximation, which was originally introduced for rf traps by Dehmelt [3]. For this one assumes that the position coordinate of a trapped ion is composed of a rapid oscillation  $\vec{\xi}(t)$  that follows the radiofrequency, the micromotion, and a slowly varying drift motion  $\vec{R}(t)$ , also referred to as the secular motion,

$$\vec{r}(t) = \vec{R}(t) + \vec{\xi}(t). \quad (3)$$

The electric field acting on the ion is expanded in a Taylor series, which leads to the equation of motion

$$m \frac{d^2}{dt^2} \vec{R} + m \frac{d^2}{dt^2} \vec{\xi} = q \vec{E}(\vec{R}, t) + q(\vec{\xi} \vec{\nabla}) \vec{E}(\vec{R}, t). \quad (4)$$

For short times, of the order of the rf oscillation period, the first and the fourth term of Eq. 4 may be neglected. This results in a differential equation for  $\vec{\xi}(t)$  that is solved by  $\vec{\xi}(t) = -\vec{\xi}_0 \sin(\omega t)$  with  $\vec{\xi}_0 = \frac{q \vec{E}(\vec{R})}{m \omega^2}$ . This describes the micromotion of an ion in the rf field. By averaging Eq. 4 over one rf oscillation period and using the solution for  $\vec{\xi}$ , the second and third terms vanish. This leads to an equation of motion for the drift coordinate  $\vec{R}$

$$m \frac{d^2}{dt^2} \vec{R} = \vec{\nabla} V_{\text{eff}}(\vec{R}), \quad (5)$$

with an effective conservative potential

$$V_{\text{eff}}(\vec{R}) = \frac{q^2}{2m\omega^2} \langle \vec{E}(\vec{R}, t)^2 \rangle. \quad (6)$$

The angle brackets denote the time average over one oscillation period.

For the ideal two-dimensional multipole field of Eq. 1 one obtains the simple, cylindrically symmetric expression for the effective potential

$$V_{\text{eff}}(\vec{R}) = \frac{q^2 n^2 V_0^2}{4m\omega^2 R_0^2} \left( \frac{R}{R_0} \right)^{(2n-2)}. \quad (7)$$

For large  $n$  this potential increases rapidly with the increasing radius  $R$  and approximates an effective potential with a large almost field-free central region and steep walls.

The effective potential is intimately related to the ion's micromotion. In fact, from the solution for  $\vec{\xi}(t)$  it follows that the time-averaged kinetic energy of the micromotion equals exactly the effective potential

$$V_{\text{eff}}(\vec{R}) = \left\langle \frac{1}{2} m \dot{\vec{\xi}}^2 \right\rangle. \quad (8)$$

This shows that within the effective potential approximation confinement in the ion trap occurs, because kinetic energy of the drift motion is reversibly converted into kinetic energy of the micromotion, leading to a maximum radius  $R_{\text{max}}$  of the ion's drift motion.

## 2.2. Stable operating conditions

The effective potential description breaks down when the amplitude of the micromotion becomes too large for the truncated Taylor expansion to be a valid approximation. In this case energy exchange between the micromotion and the secular motion occurs that increases the amplitude of the secular motion until the ion is lost in a collision with the trap electrodes. This coupling is important when the electric field amplitude changes significantly over the distance traveled by an ion during one cycle of the micromotion, i.e. when the stability parameter, introduced by Tely and Gerlich [31, 11],

$$\eta = \frac{|2(\vec{\xi}_0 \vec{\nabla}) \vec{E}(\vec{R})|}{|\vec{E}(\vec{R})|} = \frac{2|q|}{m\omega^2} \left| \vec{\nabla} |\vec{E}(\vec{R})| \right| \quad (9)$$

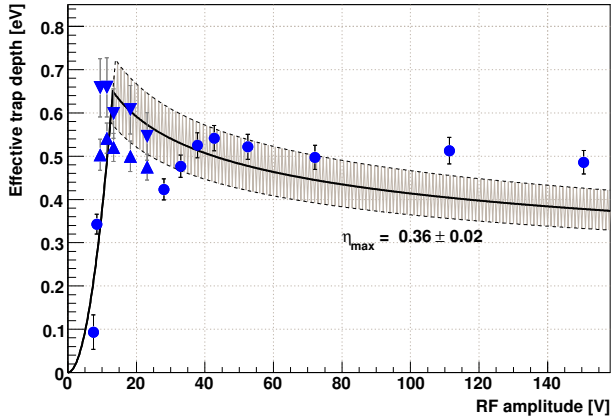


**Figure 2.** (Color online) Experimentally deduced effective depth of a 22-pole ion trap for  $\text{Cl}^-$  anions as a function of the rf amplitude. Each data point originates from a Boltzmann fit to temperature-dependent loss rates. The breakoff of the effective trap depths quadratic increase is attributed to the appearance of nonadiabatic ion motion in the trap. The solid line is a fit of a simple analytical model of the switch between adiabatic and nonadiabatic motion with the maximum stability parameter  $\eta_{\max}$  as the only free parameter [47].

is no longer a small quantity. For an ideal multipole one obtains

$$\eta = 2n(n-1) \frac{|q|V_0}{m\omega^2 R_0^2} \left( \frac{R}{R_0} \right)^{n-2}. \quad (10)$$

Note that  $\eta$  depends explicitly on the radius of the secular motion for  $n > 2$ . Only for a quadrupole ion trap one obtains a constant value, which in this case equals the parameter  $q$  that enters into the Mathieu differential equation [1, 10]. The solutions of the Mathieu equations yield the  $q$ -intervals for stable and unstable ion trapping. In multipole ion traps a clear distinction between stable and unstable regimes of trap operation is not possible [44, 45]. Instead numerical simulations have been used to define stable operating conditions:  $\eta < 0.3$  for  $R/R_0 < 0.8$  [46, 11].

An experimental test of the stability condition in a multipole ion trap has been carried out by studying the loss rate of ions from a 22-pole ion trap [48, 47]. The loss rate was found to depend exponentially on an activation energy that was associated with an effective depth of the trapping potential. The measured effective trap depth as a function of the rf amplitude is shown in Fig. 2. It follows Eq. 7 with  $R = R_0$  for low amplitudes (with no free parameter). Above 13 V the trap depth does not increase further, which indicates that for large values of  $R$   $\eta$  is too large to provide stable trapping. Numerical simulations [47] show that if an ion finds itself at positions in the trap with such a large  $\eta$ -value, the effective potential approximation breaks down and the secular kinetic energy of trapped ions is increased in the radiofrequency field. This *instability heating* then leads to trap loss.

A simple evaporation model is used to describe the leveling-off of the measured effective potential. It assumes a sudden change from stable to unstable motion at a critical radius where  $\eta$  becomes larger than a critical value. This value is determined from a fit to the data to be  $0.36 \pm 0.02$  [47], in agreement with the safe operating

conditions defined above. The model for the effective trap depth strongly simplifies the complex non-linear dynamics. Nevertheless, it provides direct experimental evidence for the range of applicability of the effective potential approximation in multipole ion traps.

### 3. Preparing cold ions

#### 3.1. Buffer gas cooling

The trapped ions are cooled in collisions with an inert buffer gas at a well-controlled temperature. Typically helium is chosen as buffer gas, because of its high vapor pressure at low temperature. The buffer gas equilibrates with the gas inlet tubes and the copper housing of the ion trap to its temperature.

The standard model to estimate collision rates of ions with neutral atoms or molecules is the Langevin or capture model [49]. The assumption of this model is that a collision occurs with 100% probability when the two collision partners come closer to each other than a critical distance. The impact parameter that belongs to this critical distance is defined by the requirement that the relative kinetic energy is just sufficient to surmount the centrifugal barrier at this impact parameter. For larger impact parameters the ion-neutral interaction is neglected. This simplified picture yields the Langevin cross section (in SI units)

$$\sigma = \frac{|q|}{2\epsilon_0} \sqrt{\frac{\alpha}{\mu v^2}}, \quad (11)$$

with the neutral polarizability  $\alpha$ , the reduced mass of the two-body system  $\mu$  and the relative velocity  $v$  ( $q$  is the ion charge and  $\epsilon_0$  the electric constant). In a thermal ensemble the collision rate coefficient  $k = \langle \sigma v \rangle$ , obtained by averaging over the velocity distribution, is the more relevant quantity. In the Langevin model one obtains the velocity and temperature independent rate coefficient

$$k = \frac{|q|}{2\epsilon_0} \sqrt{\frac{\alpha}{\mu}}. \quad (12)$$

An ion trapped in a buffer gas of given temperature will thermalize within a number of elastic collisions with the buffer gas. At a constant buffer gas density  $n_{\text{bg}}$  the average time between successive collisions is given by the inverse of the collision rate  $(kn_{\text{bg}})^{-1}$ . Typical values lie in the microsecond regime, given the typical values for the Langevin rate of  $10^{-9} \text{ cm}^3/\text{s}$  and for the density of  $10^{12}$  to  $10^{15} \text{ cm}^{-3}$ . The number of elastic collisions that are required for the ion velocity distribution to resemble a Maxwell-Boltzmann distribution is estimated with numerical simulations. A Monte Carlo simulation is used to calculate ion trajectories interacting with a buffer gas in free space. To simplify the problem isotropic elastic scattering collisions are assumed. Such simulations show that between three and ten collisions already lead to a distribution of the ion velocity that closely resembles a Maxwell-Boltzmann distribution. Ions that are trapped in a conservative, time-independent trapping potential also acquire a thermal velocity distribution, described by the temperature of the buffer gas, within only few buffer gas collisions.

#### 3.2. Radiofrequency heating

In the true time-dependent electric field of a radiofrequency ion trap the fast oscillatory micromotion perturbs the velocity distribution of trapped ions and hinders them to

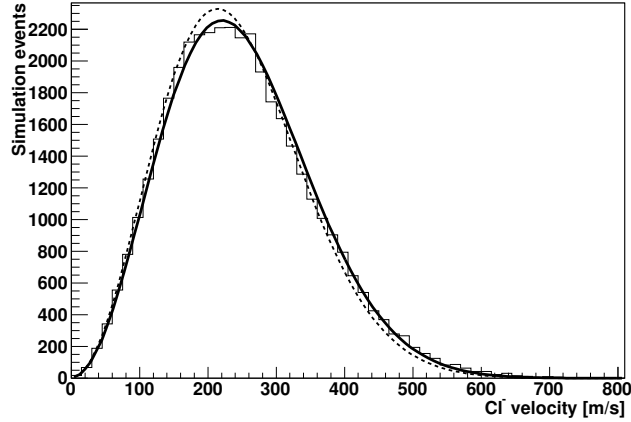


**Figure 3.** Simulated velocity distribution of  $\text{Cl}^-$  anions in a 22-pole ion trap filled with 100 K helium buffer gas. The distribution is fitted to a Maxwell-Boltzmann distribution with a translational temperature of  $106 \pm 1$  K (solid line), hotter than the buffer gas temperature due to radiofrequency heating. For comparison also the Maxwell-Boltzmann distribution for 100 K is shown (dashed line).

reach the temperature of the buffer gas. This effect of *radiofrequency heating* leads to higher translational temperatures of the trapped ions than the buffer gas temperature. In spectroscopic studies of trapped ions in 22-pole traps this effect has become visible [50, 51]. Its dependence on different parameters of the trap has recently been analyzed in detail using numerical simulations [52].

We have calculated the effect of radiofrequency heating with a Monte Carlo simulation that includes the time-dependent potential of an ideal multipole (Eq. 1). The simulation has been carried out for  $\text{Cl}^-$  in an infinitely long 22-pole ion trap ( $n = 11$ ), filled with 100 K helium buffer gas. The velocity distribution of trapped  $\text{Cl}^-$  is extracted by following the trajectory of a trapped ion and sampling its instantaneous velocity every two to three collisions with the buffer gas. This samples the thermal ion velocity distribution in the trap. The histogram in Fig. 3 shows the obtained velocity distribution for a buffer gas collision rate of  $10^5 \text{ s}^{-1}$  and an rf amplitude  $V_0 = 50$  V. The histogram is fitted with a Maxwell-Boltzmann distribution (solid line in Fig. 3) where the ions' translational temperature is the only free parameter. The numerical data agrees well with a Maxwell-Boltzmann distribution, but the obtained temperature is  $106 \pm 1$  K, about 6% hotter than the temperature of the helium buffer gas. For comparison, the dashed line shows a Maxwell-Boltzmann distribution for 100 K.

To test the numerical accuracy of the Monte-Carlo simulation we have calculated the velocity distribution for ions in the time-independent effective potential of a trap with the same trapping parameters. Here a temperature of  $101 \pm 1$  K is obtained, in agreement with the expectation of thermalization. The about 6% increase of the temperature that is found for the time-dependent radiofrequency field can therefore be attributed to radiofrequency heating. It is caused by elastic collisions with buffer gas atoms that interrupt the micromotion and thereby transfer energy from this motion into the secular motion. Therefore the temperature mismatch decreases with an



increased ratio of the ion mass to the buffer gas mass. The simulations also show that the relative temperature increase is independent of the amplitude of the radiofrequency field, the temperature and the collision rate of the buffer gas across the experimentally relevant parameter range.

The radiofrequency heating and therefore the increase of the effective ion temperature compared to the buffer gas temperature changes notably with the multipole configuration of the ion trap. The larger the multipole order  $n$  the smaller is the effective heating rate. This is qualitatively explained by the shape of the confining effective potential, which represents the kinetic energy of the micromotion. The steeper the effective potential the more time an ion spends in the almost field-free central region of the trap where buffer gas collisions may not transfer micromotion energy into the secular motion. For large  $n$ , such as in the 22-pole ion trap, radiofrequency heating can occur only near the steep wall of the effective potential.

### 3.3. Thermalization of internal degrees of freedom

For trapped molecular and cluster ions the thermalization of the translational motion to a temperature near the buffer gas temperature is only the first step. Such complex ions also possess  $3N - 6$  ( $3N - 5$  for linear molecules) internal vibrational degrees of freedom and three (two for linear molecules) rotational degrees of freedom. Inelastic collisions with the buffer gas can be employed to also thermalize these degrees of freedom.

For internal cooling, the relative kinetic energy of the ion-neutral collision system is the relevant quantity that determines the ion's internal excitation in steady state. In the case of weak radiofrequency heating the ion's translational velocity distribution follows a Maxwell-Boltzmann distribution, as discussed above. In this case the effective temperature of the relative motion is given by

$$T_{\text{eff}} = (m_n T_n + m_i T_i) / (m_n + m_i), \quad (13)$$

where  $T_n$  and  $T_i$  are the translational temperature and  $m_n$  and  $m_i$  the masses of the neutral and the ion, respectively. This shows that heavy ions and clusters in helium buffer gas may reach internal temperatures near the buffer gas temperature, even if their translational temperature is affected by radiofrequency heating. Experimentally, both rotational [53, 54] and vibrational cooling [55] have been observed.

The time scale for equilibration of the internal degrees of freedom is typically estimated to be longer than for elastic collisions, because the inelastic rate coefficient is often significantly smaller than the Langevin limit. Precise values are rare for most molecular ions, but estimates range between 10 to  $10^4$  collisions that are needed to achieve collisional thermalization. Besides this mechanism, spontaneous radiative emission may also remove internal energy from the trapped ions. This holds in particular for stiff vibrational degrees of freedom where the radiative lifetimes lie in the millisecond range [56, 57], which leads to radiative cooling rates that are comparable with collisional cooling rates.

## 4. Experimental techniques

The most widely used multipole ion trap configuration consists of  $2n$  cylindrical stainless steel electrodes that are arranged around a cylinder with inscribed radius  $R_0$  (see Fig. 1). The employed types of traps range from hexapoles and octupoles to

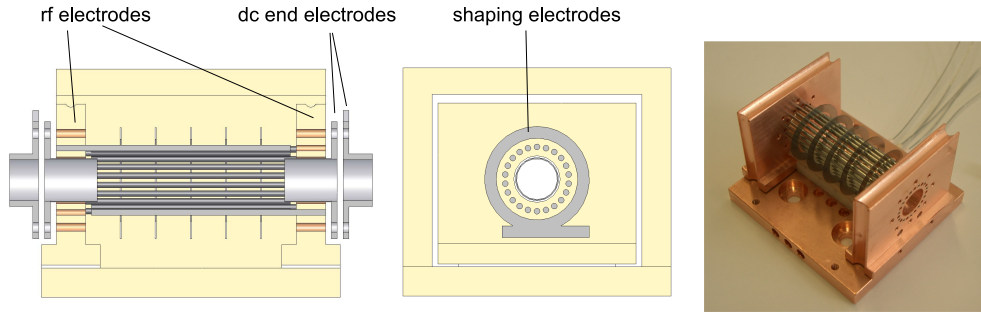


**Figure 4.** (Color online) Cross section through the center of a 22-pole ion trap [37], viewed parallel to the symmetry axis (left panel) and perpendicular to it (middle panel). On the right a photograph of the Freiburg 22-pole ion trap is shown. The 22 rf electrodes, mounted alternately into the two side plates and two pairs of dc end electrodes provide ion confinement. In addition, five shaping electrodes are placed around the 22 poles. These electrodes are used to form the trapping potential along its symmetry axis and lead to temporally shorter ion packets after extraction from the trap [47].

22-pole structures. A photograph of the 22-pole trap [37] is depicted in Fig. 4. It is about 40 mm in length with an inscribed radius of 5 mm. Confinement in the direction parallel to the electrodes is provided by two cylindrical electrostatic electrodes at the two ends of the trap.

A mechanical enclosure, typically made from copper, houses the ion trap and is filled with buffer gas for collisional cooling of the trapped ions. The trap wall temperature, which sets the buffer gas temperature, is changed by mounting the entire trap on a cryostat. Most widely used are closed-cycle helium cryostats of the Gifford McMahon type, which provide cooling powers of the order of one watt near 10 K. They are complemented with variable power resistive heaters to increase the temperature to higher values in a controlled way.

Ions are typically not formed in the cryogenic, high vacuum environment of the trap itself. Instead they are created in a separate ion source and loaded into the trap through one of the end electrodes. A variety of ion sources are used, continuous electron impact ion sources, plasma sources, radiofrequency storage ion sources, pulsed supersonic beam sources and electrospray ionization sources. Typically the ions are created with less than 1 eV kinetic energy, accelerated gently to few eV, transported through a radiofrequency quadrupole for mass selection, and then passed into the ion trap [38]. In an alternative approach, which we have developed to improve flexibility, the ions are accelerated and mass-selected by time-of-flight before the selected ion packet is decelerated and loaded into the ion trap [47]. Trapping occurs either by opening the electrostatic end electrode for the entering ions and closing it after the ions have entered the ion trap. Alternatively the ions are kept at a high enough kinetic energy to overcome the potential of the static end electrode and are then decelerated rapidly by buffer gas collisions inside the trap before they have a chance to leave the trap again. The advantage of the latter scheme is that it allows continuous loading of the ion trap over an extended period of time. This is particularly advantageous when only weak currents of the ion of interest are produced in the ion source.

About  $10^2$  to  $10^4$  trapped ions are typically used in experiments. In this case

the Coulomb interaction between the trapped ions is not significant, since the volume in which the ions are confined amounts to several  $\text{cm}^3$ . Furthermore, under these conditions the charging of insulator surfaces and saturation effects in the ion detector typically do not become important.

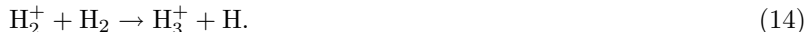
After a selected storage time, the extraction of the trapped ion ensemble proceeds by lowering the potential of one of the electrostatic end electrodes. To mass-analyze the composition of the extracted ions, either a second quadrupole mass spectrometer [38] or a second time-of-flight mass spectrometer is employed [47]. The ions are then detected with a single-particle detector, either a Daly detector [58], a channeltron detector or a microchannel plate [59]. In all cases between about 50% and more than 90% detection efficiency for single ions is obtained.

## 5. Reaction dynamics of cold ions

Many ion-molecule reactions have been studied in multipole ion traps (see e.g. Ref. [36, 38, 37, 43, 14]). In these experiments buffer gas cooling of the translational and internal degrees of freedom of the trapped ions provides the initial conditions for the chemical reactions. The neutral reagent gas is added to the trap as typically a minor constituent to an inert buffer gas such as helium. Instead of giving a full account of the recent research, the capabilities of multipole ion traps are exemplified by discussing a few selected ion-molecule reaction experiments.

### 5.1. Reactions of hydrogen molecular ions

The experimental procedure to study ion-molecule reactions is illustrated with one of the conceptually simplest bimolecular ion-molecule reactions, the hydrogen transfer reaction



With this exothermic reaction the triatomic hydrogen ion  $\text{H}_3^+$  is formed in hydrogen plasmas, one of the most important examples being cold molecular clouds in the interstellar medium. This reaction is studied by trapping  $\text{H}_2^+$  ions in a multipole ion trap and adding a controlled density  $n_{\text{H}_2}$  of  $\text{H}_2$  through a leak valve to the buffer gas in the trap. The number of  $\text{H}_2^+$  ions will then decrease and  $\text{H}_3^+$  ions will be formed as a function of storage time. By extracting all ions from the trap after different hold times and mass analyzing them one obtains data such as the one depicted in the left panel of Fig. 5. The observed exponential decay of the number  $N$  of  $\text{H}_2^+$  ions follows reaction kinetics that are described by a pseudo-first order rate equation

$$\frac{dN}{dt} = -kn_{\text{H}_2}N, \quad (15)$$

because the hydrogen density  $n_{\text{H}_2}$  stays practically constant during the experiment. Here,  $k$  is the reaction rate coefficient, the quantity of interest that characterizes the collision process. For this reaction the rate coefficient agrees well with the Langevin rate coefficient (see section 3) [60]. The probability that a reaction occurs once the two collision partners have surmounted the centrifugal barrier at long range is therefore near 100%. This shows that there is no potential barrier that could suppress this elementary chemical reaction.

The highly efficient formation of  $\text{H}_3^+$  makes it the most important molecular ion in the interstellar medium. In dense interstellar clouds it drives the formation of larger

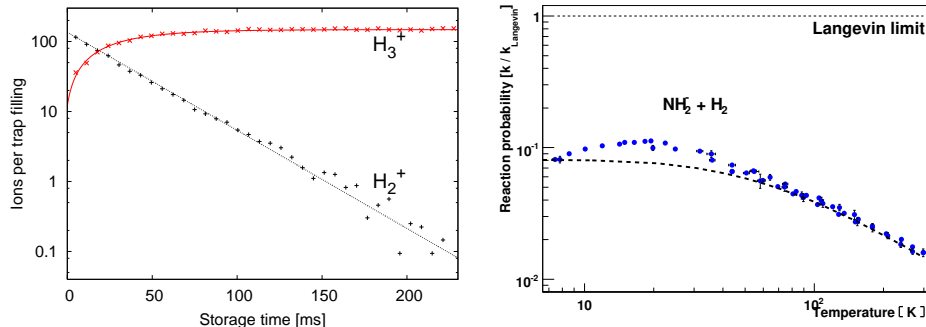


**Figure 5.** (Color online) Left panel: Dataset of a typical ion-molecule reaction measurement in a 22-pole ion trap. The measured decay of  $\text{H}_2^+$  due to reactions with neutral  $\text{H}_2$  molecules (Eq. 14) and the corresponding formation of  $\text{H}_3^+$  are shown as a function of storage time [67]. By fitting a rate coefficient model to the data (solid line) the reaction rate coefficient can be extracted. Right panel: Reaction probability, given by the ratio of the measured rate coefficient and the constant Langevin rate coefficient, for the reaction of  $\text{NH}_2^-$  with  $\text{H}_2$  (Eq. 16) as a function of temperature [13]. The data show that the probability for reaction increases with decreasing temperature but stays well below the Langevin limit. Below 20 K the data show an unexpected increase of the reaction probability that can not be explained by a classical statistical model (dashed line).

molecules by proton transfer reactions [61]. With the low temperatures of below 50 K that prevail in the dense interstellar clouds, isotopic exchange reactions of  $\text{H}_3^+$  become important. These reactions are driven by differences of the vibrational zero-point energies of hydrogen and deuterium containing molecules. Understanding these reaction rates and the influence of the rotational quantum states, which are coupled by symmetry to the molecular hyperfine states, on the reactivity still poses significant problems today [43, 62].

### 5.2. Negative ion-molecule reactions

For negative ion-molecule reactions a very different situation is found compared to the hydrogen molecular ion. A specific example is the proton transfer reaction to the negatively charged amide ion



As for most negative ion-molecule reactions [63, 64] this reaction is governed by a complex Born-Oppenheimer potential energy hypersurface [65, 13]. Specifically, the reaction has to pass two deep minima and an intermediate potential barrier on its way from reactants to products. At room temperature a reaction probability, given by the ratio of the measured rate coefficient to the calculated Langevin rate coefficient, of about 2% is found [66]. Thus, 98% of the collision events lead to back-scattering of the reactants without further reaction. This occurs despite the fact that the reaction is exothermic and also the intermediate potential barrier lies below the energy of the entrance channel. It shows that for this reaction the reaction dynamics at short range are very important.

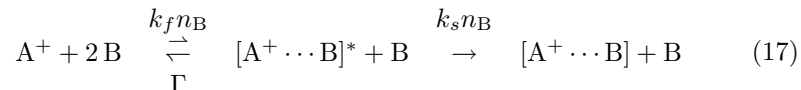
At lower temperatures the probability for reaction (16) increases strongly, as measured in a 22-pole ion trap [13]. The data are shown in right panel of Fig. 5. At 20 K the probability has increased by a factor of six. This increase is a manifestation of the complex-mediated reaction dynamics [68]: the intermediate  $\text{NH}_4^-$  complex, which is transiently formed during a collision that surmounts the centrifugal barrier, has a longer lifetime with respect to decay back to reactants at lower temperatures, because the number of available decay channels decreases. The probability to cross the intermediate potential barrier and form products, however, remains approximately constant. Therefore the overall probability to react increases.

The decrease of the reaction probability for temperatures lower than 20 K can not be explained within the classical dynamics picture of a complex-mediated reaction mechanism. Instead it is expected to represent a signature of quantum mechanical reaction dynamics in low temperature ion-molecule reactions [69].

### 5.3. Complex formation in ternary collisions

A process that connects molecular reaction dynamics with cluster physics is the association of ionic complexes upon three-body collisions. Different types of clusters have been studied in multipole ion traps, starting with experiments on the formation of hydrogen clusters  $\text{H}_5^+$  to  $\text{H}_{23}^+$  at 10 K [39]. Further ion trap experiments have investigated the temperature-dependent growth of  $(\text{CO})_n^+$  clusters for  $n = 2$  to 9 [70] and the formation of  $\text{Cl}^- \cdots \text{CH}_3\text{Cl}$  complexes [71].

The growth of ionic clusters in ternary collisions is modeled by two subsequent reaction steps:



Under the conditions in an ion trap, low buffer gas densities and long interaction times, the metastable intermediate complex is much more likely to decay back to reactants than to undergo a stabilizing collision. In this well-defined low-pressure regime the total formation rate  $R$  is given by

$$R = k_3 n_B^2, \quad (18)$$

where  $k_3$  represents the ternary rate coefficient. Typical values range between  $10^{-26}$  and  $10^{-30} \text{ cm}^6/\text{s}$ . The quadratic dependence on the neutral density is an important experimental signature of ternary collisions.

The temperature dependence of  $k_3$  provides insight into the coupling of the molecular degrees of freedom during the collisions. For many ternary collisions the temperature dependence agrees with predictions from statistical models [72]. This was also observed for the formation of trapped  $(\text{CO})_2^+$  [70]. For the growth of  $(\text{CO})_3^+$ , however, the next step in the formation of carbon monoxide clusters, deviations from the statistical model occur [70]. Also in the ternary association of chlorine anions with  $\text{CH}_3\text{Cl}$ , a large deviation was found in the temperature dependence of  $k_3$  [71]. This indicates that the molecular degrees of freedom couple differently than assumed in the statistical model. Quantum mechanical calculations may be required to clarify this.

In the low-density regime the ternary rate coefficient can be written as

$$k_3 = \frac{k_f k_s}{\Gamma} = k_f k_s \tau. \quad (19)$$

The formation rate  $k_f$  of the metastable complex is given by the Langevin collision rate for polarizable neutral species and by a modified capture rate for polar molecules. The stabilization rate  $k_s$  is the product of the capture collision rate and an, often unknown, stabilization efficiency  $\beta \leq 1$ . Thus, if  $\beta$  is known or can at least be estimated, the lifetime  $\tau = \Gamma^{-1}$  of the metastable complex  $[A^+ \cdots B]^*$  becomes experimentally accessible from measurements of the ternary rate coefficient. For the carbon monoxide clusters,  $\beta = 1$  has been assumed and lifetimes of the metastable complexes between 0.1 and 4 ns have been deduced [70] for a temperature of 80 K. For the metastable  $[Cl^- \cdots CH_3Cl]^*$  complexes,  $\beta$  was experimentally inferred to be near 1 for stabilizing collisions with  $CH_3Cl$ . This led to complex lifetimes that increased from 18 ps at 220 K to 42 ps at 150 K [71]. These experiments show that studies of trapped ions over many seconds allows one to explore molecular lifetimes that are 12 orders of magnitude shorter.

## 6. Laser spectroscopy of cold molecular ions

The preparation of molecular ions in well-defined quantum states of their rotational and vibrational motion by buffer gas cooling in multipole ion traps is very useful for precise spectroscopic studies (see e.g. Ref. [53, 73, 74, 50, 12, 55, 75, 76, 77]). However, direct absorption or fluorescence spectroscopy can not be used at number densities of  $\sim 10^3 \text{ cm}^{-3}$  [78]. Also more sensitive four-wave mixing or cavity ring-down techniques are not sensitive enough to detect photoabsorption in samples of hundreds of ions. Instead, a suitable action spectroscopy method is needed. Two schemes are most widely used, spectroscopy by chemical probing and resonant multiphoton fragmentation spectroscopy.

Action spectroscopy by chemical probing uses the fact that molecular ions are confined in the trap irrespective of their internal excitation. The internally excited molecular ion can then undergo a chemical reaction within the time set by the lifetime of the excited state, either due to radiative emission or inelastic quenching with non-reactive buffer gas. The detection of the reaction product is the signature of the absorption step. This is a sensitive spectroscopic technique, because product ions can be measured with single-particle detection efficiency. Even if no reaction occurred for a given excitation step, buffer gas cooling back to the initial internal state distribution offers subsequent chances for successful probing.

The earliest applications of chemical probing as a sensitive technique for action spectroscopy employed ion beams [79, 80] and ion flow tubes [81]. It has been applied for the first time in a multipole ion trap to electronic spectroscopy of  $N_2^+$  ions using narrow-band continuous wave laser light [53]. Here, the endothermic charge transfer reaction of  $N_2^+$  with Ar does not occur if the  $N_2^+$  ions are in the electronic and vibrational ground state and have a near-room temperature thermal population of rotation states. Once the  $N_2^+$  ions are excited to the  $A^2\Pi_u$  state and have decayed back to vibrationally excited levels in the  $X^2\Sigma_g^+$  state, the charge transfer process occurs with a finite rate coefficient and  $Ar^+$  ions are formed. After a suitable interaction time of the excitation laser with the ions, the trap is emptied and the number of produced  $Ar^+$  ions is measured. By scanning the laser frequency across the Doppler profile of the trapped ions one obtains the resonance profiles shown in the left panel of Fig. 6. Both at 410 and at 50 K the widths of the Doppler profiles are found to be in agreement with the expected width based on the denoted buffer gas temperature determined by the trap wall. This shows that in this experiment no significant radiofrequency heating

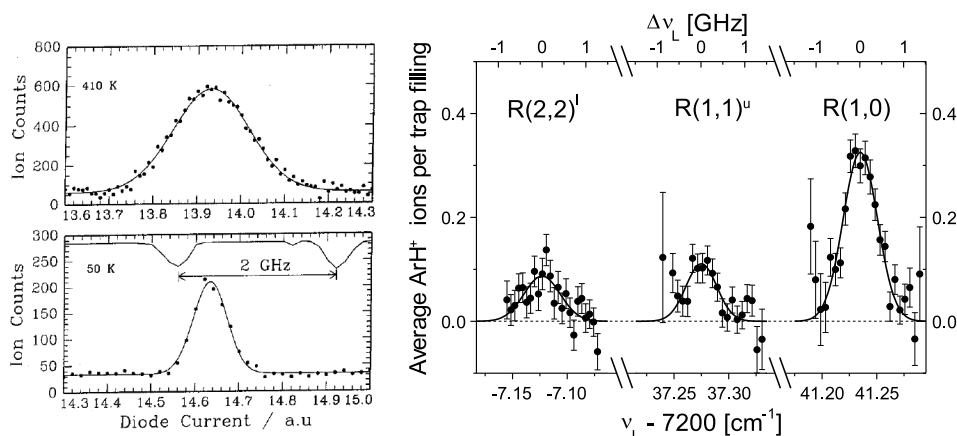


**Figure 6.** Left panel: Electronic chemical probing spectroscopy of  $N_2^+$ . The spectroscopic signature is derived by laser-induced charge transfer in collisions with argon, forming  $Ar^+$ . Two line scans are shown with the  $Ar^+$  count rate plotted as a function of laser frequency. By fitting Doppler profiles to the lines translational temperatures are obtained that agree with the applied buffer gas temperature [53] Right panel: Action spectroscopy of vibrational overtones of  $H_3^+$ , probed by proton-transfer reactions with argon atoms, which become exothermal for three quanta of vibrational excitation. Doppler-broadened lines for three different rovibrational transitions are shown [50]. Here, the rotational and translational temperatures agreed with each other, but were much larger than the buffer gas temperature, which is explained by strong rf heating [52].

occurred within the experimental accuracy.

An alternative chemical probing scheme has been applied to high resolution infrared overtone spectroscopy of the triatomic  $H_3^+$  ion, again using a narrow-band cw laser. Electric dipole-allowed transitions in this simplest polyatomic molecule are limited to excitations of its asymmetric stretching mode. Once more than two quanta of vibration are excited, the  $H_3^+$  ion may undergo proton transfer to Ar. The spectroscopic signature is therefore the detection of  $ArH^+$  product ions. Doppler profiles for the three lowest rotational energy levels of  $H_3^+$  ( $J, K$ ) = (1, 1), (1, 0) and (2, 2) are plotted in the right panel of Fig. 6. These data show that the ions' Doppler temperature (found here to be about  $150 \pm 20$  K) does not automatically coincide with the buffer gas temperature (set to 55 K in this experiment). This can be explained by rf heating due to  $H_3^+$ -Ar collisions, which have an unfavorable mass ratio (see section 3) [52]. This is circumvented using higher helium buffer gas densities, as shown in a recent experiment that studies high overtone excitation of  $H_3^+$  levels that lie beyond the barrier to linearity [51].

Many more molecules have been studied with infrared chemical probing spectroscopy, such as deuterated variants of  $H_3^+$  [76, 82],  $C_2H_2^+$  [73] and  $CH_5^+$  [12]. In the experiment on  $CH_5^+$ , the use of the infrared free electron laser FELIX has allowed for an investigation of the very floppy low-frequency bending vibrations. Besides yielding structural information these chemical probing experiments may also reveal quantum-state specific rate coefficients for the reaction that is induced by the laser. This has already been used in Ref. [73] to study the influence of the rotational quantum state on the reactivity.

The second scheme for action spectroscopy of trapped ions is resonant multiphoton fragmentation spectroscopy. It is widely applied in the near-visible range, typically using nanosecond pulsed lasers. It can be applied to a large number of ions that have low-lying excited electronic states, in particular many organic molecules. Here the energy of two or three photons is sufficient to fragment the molecule. With the first photon a specific resonance is excited in the molecular ion that is studied by mass-spectrometrically detecting the photofragments that are created after the absorption of the additional photons. This approach is leading to new insight into large carbon containing molecules [83], which may be responsible for some of the unidentified diffuse interstellar bands, a long standing problem in laboratory astrophysics [84]. Furthermore, rapid progress is being made in the understanding of the structure of protonated amino acids, bare and micro-solvated with a few water molecules [55, 85]. Spectroscopic experiments have also been carried out on pure water clusters, where the spectroscopic signature of fragmentation is already achieved by the absorption of a single infrared photon [86].

Multipole ion traps have also recently led to precise studies of the photodetachment of trapped negative ions in a laser field [87]. Here the absorption of a single visible or near-ultraviolet photon induced the detachment process  $A^- + h\nu \rightarrow A + e^-$ . This leads to a loss rate for the trapped anions. By scanning the entire ion density distribution with the photodetachment laser beam, the absolute total photodetachment cross section can be extracted from the density-dependent loss rate (see Ref. [88] for more details). This allows one to derive absolute cross sections with high accuracy independent of any theoretical model. About 5% relative accuracy have been achieved for the  $O^-$  and  $OH^-$  cross sections in this way [89]. These data are not only benchmarks for high-level quantum calculations, they are also important parameters for modeling the negative ion composition in the Earth's atmosphere or the stability of interstellar negative ions [90, 91].

## 7. Outlook

Multipole ion traps are versatile tools to study different molecular processes, in particular the 22-pole ion trap is being used in many experiments. Recently a lot of progress is made in the understanding of the dynamics of ions in multipole ion traps. Cooling and radiofrequency heating of trapped ions in the buffer gas has recently been studied [52]. The density distribution of trapped ions and thus the effective potential of multipole traps can now be visualized using photodetachment tomography [88]. With this knowledge new, improved designs of ion traps may be anticipated.

New technologies for the fabrication of radiofrequency ion traps on planar chip structures are already being explored extensively [92, 93, 94, 95, 96, 97, 98, 99]. We have recently developed a high-order multipole ion trap which is based on two planar microstructured chips (see Fig. 7) [100] and which successfully traps ions for many seconds [101]. Here 32 radiofrequency and several electrostatic electrodes are etched out of a gold layer on top of the two glass substrates. The goal of lower ion temperatures may be reached with colder helium cryostats or possibly with non-thermal buffer gas from the tail of an effusive beam. Laser-cooled atoms could in the future also be used to collisionally cool ions to much lower temperatures than the current limit of around 4 K.

Future experiments with the cold ions in multipole ion traps may search for quantum scattering or Feshbach resonances and their possible control with external



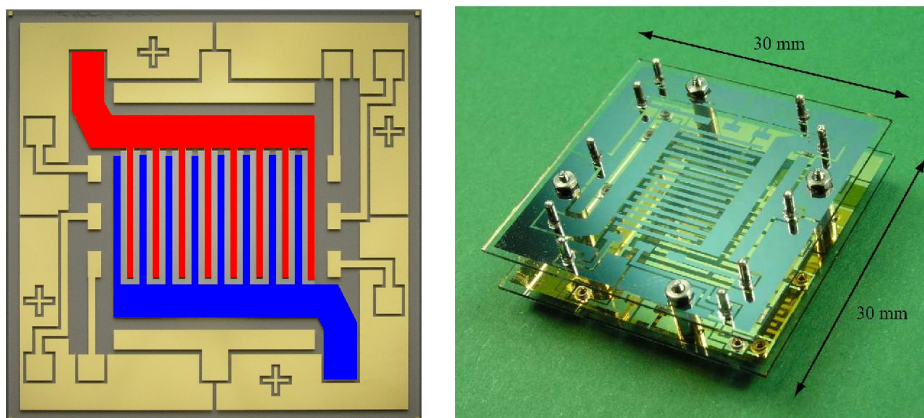


**Figure 7.** (Color online) Left panel: view of one of the chips of a planar multipole ion trap [100]. The gold electrodes that are connected to the two phases of the confining radiofrequency mirror are colored in red and blue; they provide a repulsive effective potential “mirror” in front of the chip surface. Static potentials are applied to the additional electrodes on the chip in order to confine ions in all three dimensions. Right panel: photograph of an assembled chip-based planar multipole ion trap fabricated with  $2 \times 16$  etched gold electrodes on two glass substrates, 5 mm apart. Ions are confined in the space between the two chips [101].

fields [102, 103, 104]. They may resolve the details of the rotational and hyperfine couplings in isotopic substitution reactions of “simple” hydrogen molecular ions. And they may cover processes that have recently been identified as important in interstellar space, such as reactions of atomic species such as hydrogen, carbon or oxygen or reactions of negatively charged molecular ions [105].

The translationally and internally cold molecular ions that are prepared in a multipole ion trap are also ideal for experiments that are carried out with other experimental techniques. 22-pole ion traps are already employed as a source at the electrostatic storage ring ELISA and the magnetic heavy ion storage ring TSR [106]. They also allow to prepare cold metal clusters for photoelectron imaging studies [107]. In the future they may be used for low-energy collision experiments of molecular ions and clusters in a crossed-beam imaging spectrometer [108, 109].

The spectroscopy with cold trapped molecular ions will expand with respect to the systems studied and with respect to the employed frequency range of the exciting radiation. The application of infrared and optical spectroscopy will continue to give insight into vibrational and electronic transitions of linear and cyclic organic molecules and in protonated polypeptides. In a pioneering experiment pure rotational transitions excited with terahertz radiation have been studied in trapped  $\text{H}_2\text{D}^+$  [110]. In addition, new ultraviolet and x-ray sources, such as the free-electron lasers, may allow for new types of experiments with cold, trapped molecular ions.

## Acknowledgments

This article reviews work that the author has been fortunate to carry out with many colleagues. In particular collaboration with Jochen Mikosch, Sebastian Trippel,

Rico Otto, Petr Hlavenka, Ulrike Frühling, Raphael Berhane, Christoph Eichhorn, Dirk Schwalm, and Matthias Weidemüller is gratefully acknowledged. We thank Dieter Gerlich for his advice on 22-pole traps and Oskar Asvany and Stephan Schlemmer for many discussions on ion trapping. Our research has been supported by the Eliteförderung der Landesstiftung Baden-Württemberg and by the Deutsche Forschungsgemeinschaft.

## References

- [1] Paul W, Osberghaus O and Fischer E 1958 *Forschungsber. Wirtsch.-Verkehrsminist. Nordrhein-Westfalen* **415**
- [2] Paul W 1990 *Rev. Mod. Phys.* **62** 531
- [3] Dehmelt H G 1967 *Adv. At. Mol. Phys.* **3** 53
- [4] Zajfman D, Heber O, Vejby-Christensen L, Ben-Itzhak I, Rappaport M, Fishman R and Dahan M 1997 *Phys. Rev. A* **55** 1577
- [5] Hu Q Z, Noll R J, Li H Y, Makarov A, Hardman M and Cooks R G 2005 *J. Mass Spectrom.* **40** 430
- [6] Blaum K 2006 *Phys. Rep.* **425** 1–78
- [7] Douglas D J, Frank A J and Mao D 2005 *Mass Spectrom. Rev.* **24** 1
- [8] Margolis H S, Barwood G P, Huang G, Klein H A, Lea S N, Szymaniec K and Gill P 2004 *Science* **306** 1355–1358
- [9] Rosenband T, Hume D B, Schmidt P O, Chou C W, Brusch A, Lorini L, Oskay W H, Drullinger R E, Fortier T M, Stalnaker J E, Diddams S A, Swann W C, Newbury N R, Itano W M, Wineland D J and Bergquist J C 2008 *Science* **319** 1808–1812
- [10] Leibfried D, Blatt R, Monroe C and Wineland D 2003 *Rev. Mod. Phys.* **75** 281
- [11] Gerlich D 1992 *Adv. Chem. Phys.* **82** 1
- [12] Asvany O, Kumar P, Redlich B, Hegemann I, Schlemmer S and Marx D 2005 *Science* **309** 1219–1222
- [13] Otto R, Mikosch J, Trippel S, Weidemüller M and Wester R 2008 *Phys. Rev. Lett.* **101** 063201
- [14] Gerlich D and Smith M 2006 *Phys. Scripta* **73** C25
- [15] Grimm R, Weidemüller M and Ovchinnikov Y B 2000 *Adv. At. Mol. Opt. Phys.* **42** 95–170
- [16] Neuhauser W, Hohenstatt M, Toschek P and Dehmelt H 1978 *Phys. Rev. Lett.* **41** 233–236 ISSN 0031-9007
- [17] Roth B and Schiller S 2008 *arXiv:0812.1154v1*
- [18] Mølhave K and Drewsen M 2000 *Phys. Rev. A* **62** 011401(R)
- [19] Drewsen M, Mortensen A, Martinussen R, Staunum P and Sørensen J L 2004 *Phys. Rev. Lett.* **93** 243201
- [20] Blythe P, Roth B, Fröhlich U, Wenz H and Schiller S 2005 *Phys. Rev. Lett.* **95** 183002
- [21] Bertelsen A, Vogelius I S, Jorgensen S, Kosloff R and Drewsen M 2004 *Eur. Phys. J. D* **31** 403
- [22] Højbjerg K, Offenbergh D, Bisgaard C Z, Stapelfeldt H, Staunum P F, Mortensen A and Drewsen M 2008 *Phys. Rev. A* **77** 030702
- [23] Koелеmeij J C J, Roth B, Wicht A, Ernsting I and Schiller S 2007 *Phys. Rev. Lett.* **98** 173002
- [24] Bertelsen A, Jorgensen S and Drewsen M 2006 *J. Phys. B* **39** L83–L89
- [25] Koелеmeij J C J, Roth B and Schiller S 2007 *Phys. Rev. A* **76** 023413
- [26] Vogelius S, Madsen L B and Drewsen M 2002 *Phys. Rev. Lett.* **89** 173003
- [27] Staunum P, Højbjerg K, Wester R and Drewsen M 2008 *Phys. Rev. Lett.* **100** 243003
- [28] Roth B, Offenbergh D, Zhang C B and Schiller S 2008 *Phys. Rev. A* **78** 042709
- [29] Willitsch S, Bell M T, Gingell A D, Procter S R and Softley T P 2008 *Phys. Rev. Lett.* **100** 043203
- [30] Willitsch S, Bell M T, Gingell A D and Softley T P 2008 *Phys. Chem. Chem. Phys.* **10** 7200
- [31] Teloy E and Gerlich D 1974 *Chem. Phys.* **4** 417
- [32] Armentrout P B 2001 *Annu. Rev. Phys. Chem.* **52** 423
- [33] Schubert M, Siemers I and Blatt R 1989 *J. Opt. Soc. Am. B* **6** 2159
- [34] Walz J, Siemers I, Schubert M, Neuhauser W, Blatt R and Teloy E 1994 *Phys. Rev. A* **50** 4122
- [35] Okada K, Yasuda K, Takayanagi T, Wada M, Schuessler H A and Ohtani S 2007 *Phys. Rev. A* **75** 033409
- [36] Gerlich D and Kaefer G 1989 *Ap. J.* **347** 849
- [37] Gerlich D 1995 *Phys. Scripta* **T59** 256
- [38] Gerlich D and Horning S 1992 *Chem. Rev.* **92** 1509

- [39] Paul W, Lücke B, Schlemmer S and Gerlich D 1995 *Int. J. Mass Spectrom.* **150** 373–387
- [40] Paul W, Schlemmer S, Lücke B and Gerlich D 1996 *Chem. Phys.* **209** 265–274
- [41] Gerlich D 2003 *Hyperf. Int.* **146/147** 293
- [42] Gerlich D 2008 *Low temperatures and cold molecules* ed Smith I W M (World Scientific Publishing)
- [43] Gerlich D, Herbst E and Roueff E 2002 *Planetary and Space Science* **50** 1275
- [44] Haegg C and Szabo I 1986 *Int. J. Mass Spectrom.* **73** 237
- [45] Haegg C and Szabo I 1986 *Int. J. Mass Spectrom.* **73** 277
- [46] Gerlich D 1986 *Electronic and Atomic Collisions* ed Lorents D C (Elsevier, Amsterdam) p 541
- [47] Mikosch J, Frühling U, Trippel S, Otto R, Hlavenka P, Schwalm D, Weidemüller M and Wester R 2008 *Phys. Rev. A* **78** 023402
- [48] Mikosch J, Frühling U, Trippel S, Schwalm D, Weidemüller M and Wester R 2007 *Phys. Rev. Lett.* **98** 223001
- [49] Levine R D 2005 *Molecular Reaction Dynamics* (Cambridge University Press)
- [50] Mikosch J, Kreckel H, Wester R, Plasil R, Glosik J, Gerlich D, Schwalm D and Wolf A 2004 *J. Chem. Phys.* **121** 11030
- [51] Kreckel H, Bing D, Reinhardt S, Petrigiani A, Berg M and Wolf A 2008 *J. Chem. Phys.* **129** 164312
- [52] Asvany O and Schlemmer S 2009 *Int. J. Mass Spectrom.* **279** 147
- [53] Schlemmer S, Kuhn T, Lescop E and Gerlich D 1999 *Int. J. Mass Spectrom.* **185-187** 589
- [54] Dzhonson A, Gerlich D, Bieske E J and Maier J P 2006 *J. Mol. Struct.* **795** 93
- [55] Boyarkin O V, Mercier S R, Kamariotis A and Rizzo T R 2006 *J. Am. Chem. Soc.* **128** 2816
- [56] Amitay Z, Baer A, Dahan M, Knoll L, Lange M, Levin J, Schneider I F, Schwalm D, Suzor-Weiner A, Vager Z, Wester R, Wolf A and Zajfman D 1998 *Science* **281** 75–8
- [57] Hechtfisher U, Amitay Z, Forck P, Lange M, Linkemann J, Schmitt M, Schwalm D, Wester R, Zajfman D and Wolf A 1998 *Phys. Rev. Lett.* **80** 2809–12
- [58] Daly N R 1960 *Rev. Sci. Instrum.* **31** 264
- [59] Wiza J L 1979 *Nucl. Instrum. Methods* **162** 587
- [60] Glenewinkel-Meyer T and Gerlich D 1997 *Israel Journal of Chemistry* **37** 343
- [61] Smith D and Spanel P 1995 *Mass Spectrom. Rev.* **14** 255
- [62] Hugo E, Asvany O and Schlemmer S 2009 *J. Chem. Phys.* **submitted**
- [63] DePuy C H 2000 *Int. J. Mass Spectrom.* **200** 79–96
- [64] Laehdahl J K and Uggeruk E 2002 *Int. J. Mass Spectrom.* **214** 277
- [65] Kremer D and Kraka E 1986 *Chem. Phys. Lett.* **131** 507
- [66] Bohme D K, Hemsworth R S and Rundle H W 1973 *J. Chem. Phys.* **59** 77
- [67] Asvany O 2009 Private communication
- [68] Troe J 1994 *J. Chem. Soc. Far. Trans.* **90** 2303
- [69] Dashevskaya E I, Litvin I, Nikitin E E and Troe J 2005 *J. Chem. Phys.* **122** 184311
- [70] Schlemmer S, Luca A, Glosik J and Gerlich D 2002 *J. Chem. Phys.* **116** 4508–4516
- [71] Mikosch J, Otto R, Trippel S, Eichhorn C, Weidemüller M and Wester R 2008 *J. Phys. Chem. A* **112** 10448
- [72] Viggiano A A 1986 *J. Chem. Phys.* **84** 244
- [73] Schlemmer S, Lescop E, von Richtofen J, Gerlich D and Smith M A 2002 *J. Chem. Phys.* **117** 2068
- [74] Asmis K R, Pivonka N L, Santambrogio G, Brümmer M, Kaposta C, Neumark D M and Wöste L 2003 *Science* **299** 1375
- [75] Dzhonson A and Maier J P 2006 *Int. J. Mass Spectrom.* **255** 139–143
- [76] Glosik J, Hlavenka P, Plašil R, Windisch F, Gerlich D, Wolf A and Kreckel H 2006 *Phil. Trans. R. Soc. A* **364** 2931
- [77] Janssens E, Santambrogio G, Brümmer M, Wöste L, Lievens P, Sauer J, Meijer G and Asmis K R 2006 *Phys. Rev. Lett.* **96** 233401
- [78] Saykally R J 1988 *Science* **239** 157
- [79] Carrington A, Milverton D R J and Sarre P J 1978 *Mol. Phys.* **35** 1505
- [80] Wing W H, Ruff G A, Lamb J W E and Spezeski J J 1976 *Phys. Rev. Lett.* **36** 1488
- [81] Grieman F J, Hansen J C and Moseley J T 1982 *Chem. Phys. Lett.* **85** 53
- [82] Asvany O, Hugo E, Müller F, Kühnemann F, Schiller S, Tennyson J and Schlemmer S 2007 *J. Chem. Phys.* **127** 154317
- [83] Jochowitz E B and Maier J P 2008 *Annu. Rev. Phys. Chem.* **59** 519–544
- [84] Sarre P J 2006 *J. Mol. Spectrosc.* **238** 1
- [85] Mercier S R, Boyarkin O V, Kamariotis A, Guglielmi M, Tavernelli I, Cascella M, Rothlisberger U and Rizzo T R 2006 *J. Am. Chem. Soc.* **128** 16938

- [86] Wang Y S, Tsai C H, Lee Y T, Chang H C, Jiang J C, Asvany O, Schlemmer S and Gerlich D 2003 *J. Phys. Chem. A* **107** 4217–4225
- [87] Trippel S, Mikosch J, Berhane R, Otto R, Weidemüller M and Wester R 2006 *Phys. Rev. Lett.* **97** 193003
- [88] Otto R, Hlavenka P, Trippel S, Mikosch J, Singer K, Weidemüller M and Wester R 2009 *J. Phys. B special issue on ion trapping submitted*
- [89] Hlavenka P, Otto R, Trippel S, Mikosch J, Weidemüller M and Wester R 2009 *J. Chem. Phys.* **in press**
- [90] McCarthy M C, Gottlieb C A, Gupta H and Thaddeus P 2006 *Astrophys. J. Lett.* **652** L141
- [91] Brünken S, Gupta H, Gottlieb C A, McCarthy M C and Thaddeus P 2007 *Astrophys. J. Lett.* **664** L43
- [92] Madsen M J, Hensinger W K, Stick D, Rabchuk J A and Monroe C 2004 *Appl. Phys. B* **78** 639
- [93] Blain M G, Riter L S, Cruz D, Austin D E, Wu G, Plass W R and Cooks R G 2004 *Int. J. Mass Spectrom.* **236** 91
- [94] Stick D, Hensinger W K, Olmschenk S, Madseb M J, Schwab K and Monroe C 2006 *Nature Physics* **2** 36
- [95] Pearson C E, Leibbrandt D R, Bakr W S, Mallard W J, Brown K R and Chuang I L 2006 *Phys. Rev. A* **73** 032307
- [96] Schulz S, Poschinger U, Singer K and Schmidt-Kaler F 2006 *Fortschr. Phys.* **54** 648
- [97] Seidelin S, Chiaverini J, Reichle R, Bollinger J J, Leibfried D, Britton J, Wesenberg J H, Blakestad R B, Epstein R J, Hume D B, Itano W M, Jost J D, Langer C, Ozeri R, Shiga N and Wineland D J 2006 *Phys. Rev. Lett.* **96** 253003
- [98] Pau S, Pai C S, Low Y L, Moxom J, Reilley P T A, Whitten W B and Ramsey J M 2006 *Phys. Rev. Lett.* **96** 120801
- [99] Amini J M, Britton J, Leibfried D and Wineland D J 2008 *arXiv:0812.3907v1*
- [100] Kröner M, Debatin M, Mikosch J, Trippel S, Just E, Reetz-Lamour M, Wester R, Weidemüller M and Woias P 2007 *Proceedings of the Transducers and Eurosensors '07*
- [101] Debatin M, Kröner M, Mikosch J, Trippel S, Morrison N, Reetz-Lamour M, Woias P, Wester R and Weidemüller M 2008 *Phys. Rev. A* **77** 033422
- [102] Bodo E, Scifoni E, Sebastianelli F, Gianturco F A and Dalgarno A 2002 *Phys. Rev. Lett.* **89** 283201
- [103] Stoecklin T and Voronin A 2005 *Phys. Rev. A* **72** 042714
- [104] Cote R and Dalgarno A 2000 *Phys. Rev. A* **62** 012709
- [105] Millar T J, Walsh C, Cordiner M A, Chuimín R N and Herbst E 2007 *Astrophys. J.* **662** L87
- [106] Kreckel H, Motsch M, Mikosch J, Glosik J, Plasil R, Altevogt S, Andrianarijaona V, Buhr H, Hoffmann J, Lammich L, Lestinsky M, Nevo I, Novotny S, Orlov D A, Pedersen H B, Sprenger F, Terekhov A S, Toker J, Wester R, Gerlich D, Schwalm D, Wolf A and Zajfman D 2005 *Phys. Rev. Lett.* **95** 263201
- [107] Bartels C, Hock C, Huwer J, Kuhn R, Schwöbel J and von Issendorff B 2009 *Science* **in press**
- [108] Mikosch J, Frühling U, Trippel S, Schwalm D, Weidemüller M and Wester R 2006 *Phys. Chem. Chem. Phys.* **8** 2990
- [109] Mikosch J, Trippel S, Eichhorn C, Otto R, Lourderaj U, Zhang J X, Hase W L, Weidemüller M and Wester R 2008 *Science* **319** 183
- [110] Asvany O, Ricken O, Müller H S P, Wiedner M C, Giesen T F and Schlemmer S 2008 *Phys. Rev. Lett.* **100** 233004